Glycidol hydrogenolysis on a cheap mesoporous acid saponite supported Ni catalyst as alternative approach to 1,3-propanediol synthesis

F. B. Gebretsadik[a], J. Ruiz-Martinez[b], P. Salagre*[, a], Y. Cesteros[a]

[a] *Departament de Química Física i Inorgànica, Universitat Rovira i Virgili, C/ Marcel·lí Domingo s/n, 43007 Tarragona, Spain.*

[b] *Inorganic Chemistry and Catalysis, Debye Institute of Nanomaterials, Utrecht University, Universiteitsweg 99, 3584 CG Utrecht, The Netherlands*

*Corresponding author

Dr. Pilar Salagre

Universitat Rovira i Virgili, Dpt.Quimica Fisica i Inorgànica

C/Marcel·lí Domingo s/n, 43007 Tarragona, Spain

Tel: +34 977559571; Fax: +34 977559563

E-mail: pilar.salagre@urv.cat

Abstract

This study explores the use of glycidol, as alternative to glycerol, to improve the selectively to 1,3-propanediol (PrD) by hydrogenolysis. The reaction was performed using Ni (with different Ni wt %) supported on an acid delaminated saponite catalysts which are cheaper compared to the expensive catalysts needed to favor the 1,3-PrD formation by glycerol hydrogenolysis. An increase in metallic area and a decrease in the catalyst acidity resulted in higher conversion and selectivity to propanediols (1,2- + 1,3-PrD). An acid activation of glycidol during hydrogenolysis promoted the 1,3-PrD formation and increased the 1,3-PrD/1,2-PrD ratio. For the catalyst prepared with 40 wt % Ni loading, an increase in the reaction temperature to 423 and 453 K led to higher 1,3-PrD/1,2-PrD ratio. The highest 1,3-PrD yield (29%) and 1,3-PrD/1,2-PrD ratio (0.97) at total conversion were obtained at 453 K, after 1 h. The overall 1,3-PrD yield from glycerol, assuming a two-step synthesis (Glycerol → Glycidol → 1,3-PrD) and a yield of 78% for the first step, should be around 23%. This value is comparable to that reported for the hydrogenolysis of glycerol using noble metal catalysts.

Keywords: glycidol; hydrogenolysis; propanediols; saponites; bifunctional catalysis.

1. INTRODUCTION

Increased environmental awareness, the depletion and non-renewable nature of petroleum and geopolitical issues initiated the oil and petrochemical industry to look for other renewable options [1, 2]. Consequently, biodiesel production has become interesting to supply renewable liquid fuel and raw materials [3]. During biodiesel production, glycerol is co-produced in 10 wt % yield [4-6] and its over supply decreases its market value. Hence, in order to make the biodiesel production economically feasible, glycerol should be transformed to high-added value chemicals. One approach is to hydrogenolyze it to 1,2- and 1,3-propanediol (PrD). 1,2-PrD is a precursor of polyethers, unsaturated polyester resins, hydraulic fluids and antifreeze products [7-10]. The synthesis of 1,3-PrD is engaging because it is used in polypropylene terephthalate (PPT) production [11], a polymer that displays unique properties [12, 13] and current industrial processes for 1,3-PrD production are costly [14].

Direct hydrogenolysis of glycerol to PrDs has been extensively studied; the main products, in most cases, are the less valuable 1,2-PrD and propanols [15]. Bacterial fermentation of glycerol gave 1,3-PrD with high selectivity [16-18]. Nevertheless, the reaction proceeds slowly in two steps with low product concentration [19]. Several homogeneous catalysts based on Pd, Rh and Ru complexes and various acid co-catalysts have been patented or reported for this reaction [20-22].

Various heterogeneous catalysts were tested for the reduction of glycerol to 1,3-PrD. Rh/SiO_2 catalyst with H_2WO_4 as co-catalyst gave 1,3-PrD in 4 % yield at 473 K and 8 MPa hydrogen pressure [23]. Kurosaka et al. carried out the reduction of glycerol at 453 K, 8 MPa H_2 pressure and in 1,3-dimethyl-2-imidazolidone using a Pt/WO_3/ZrO_2 catalyst and obtained 1,3-PrD in 24 % yield [19]. Recently, Tomishige

group reported a series of supported Rh and Ir catalysts modified with ReO_x and co-catalyzed by various mineral and solid acids [24-26]. The authors claimed that in the best case, 1,3-PrD was obtained in 38 % yield, which is the highest reported in the literature. Huang et al. described the vapor phase reduction of glycerol using Cu/SiO_2 in the presence of $H_4SiW_{12}O_{40}$ as an acid co-catalyst [27]. The reaction, performed at 483 K and 0.54 MPa hydrogen pressure, gave 83 % conversion with 31.2 % and 22.2 % selectivity to 1,3-PrD and 1,2-PrD, respectively.

In general, many of the heterogeneous and homogeneous catalytic systems reported in the literature for the hydrogenolysis of glycerol to 1,3-PrD involve expensive noble metals, such as Pt, Ir, Rh and Pd [19, 24, 27, 28]. Moreover, the reaction involve high temperature and/or pressure, long reaction time and selectivity and yield to 1,3-PrD in most cases were low [17, 29]. In order to enhance the 1,3-PrD selectivity and yield, other approaches involving protective group chemistry [30] and toxic acrolein intermediates [31] have been proposed. These reactions resulted in 1,3-PrD yields of 72 and 60 %, respectively.

Looking for alternatives to glycerol to obtain 1,3-PrD, glycidol could be a good candidate. Glycidol can be catalytically synthesized from glycerol with high yields (72-78 %) [32-35]. Although there are no literature records for glycidol reduction to 1,3-PrD, hydrogenolysis and isomerization of related compounds has been reported [36-41]. Various substituted epoxides were isomerized to aldehydes or ketones using solid acid catalysts [36-38] and their hydrogenolysis was carried out on supported metal catalysts [39-41]. Acid catalysed ring opening reaction followed by metal catalysed hydrogenation of tetrahydrofurfuryl alcohol was proposed using ReO_x-promoted Rh/C [42] and Ir–ReO_x/SiO_2 catalysts [43] with good conversion (> 47 %) and high selectivity to 1,5 pentanediol (97 %). The presence of Brønsted acid

functionality in the catalysts was claimed to have a role in selective cleavage of the more substituted C-O bond in the ring leading to terminal diols [38, 42, 43].

In this study, we propose the use of glycidol as an alternative to glycerol to produce 1,3-PrD by hydrogenolysis (Scheme 1), using cheap non-noble, Ni metal catalysts supported on Brønsted acid saponites. The effect of acidity of the support, reaction temperature, Ni loading and reaction time were studied and optimized.

2. EXPERIMENTAL

2.1. Preparation of nickel catalysts supported on saponites

Supported Ni catalysts were prepared by incipient wetness impregnation of a mesoporous H^+-saponite, labelled as Sap. The saponite was prepared following a method previously reported by our research group [44]. Sap was prepared from slurry of initial pH 13, in a presence of surfactant (dodecyltrimethylammonium chloride) as template and using microwaves in the aging treatment. The BET area, average pore and acidity values of the resulting saponite (Sap) are shown between parentheses in Table 1. The Na-form (Sap*) was also used as support in one of the catalysts in order to decrease its acidity [44].

For catalyst preparation, 1 g of support (Sap) was kept in a round bottom flask and 0.5 M nickel nitrate solution in ethanol was used to prepare catalysts with 15, 30 and 40 wt % Ni loading. The solvent was removed by rotary evaporation, samples were dried in an oven at 363 K overnight and calcined at 723 K for 5 h. It was then reduced in a tubular reactor under hydrogen flow (75 mL/min) at 623 K for 6 h. The catalysts were labelled as Ni(x)/ (Sap or Sap*), where x represents the wt % of Ni loading. The letter P in the sample names stands for the catalyst precursors, which are the calcined samples before reduction.

2.2. Catalyst characterization

X-ray diffractogram (XRD) patterns of the powdered catalyst precursors (NiO/Sap) and catalysts were recorded on a Siemens D5000 diffractometer equipped with a CuKα radiation (λ =1.54 Å) source. Measurements were done in the 2θ diffraction range of 5 - 70° with an angular step of 0.05° and at rate of 3s per step. Crystalline phases were identified by cross comparison of the diffractogram of the sample with a reference data from international centre for diffraction data (JCPDS files). Integral breadth, estimated by fitting the characteristic reflection of each phase using TOPAS 4.1, was used to calculate the crystallite sizes by applying the Scherrer equation.

In-situ XRD measurement was conducted for the PNi(15)/Sap sample to confirm the formation of metallic Ni. Sample was heated in an Anton Paar XRK900 X-ray reactor chamber mounted on the diffractometer, from room temperature to 573 K at a rate of 50 K/ min under a flow of 25% H_2 in He. Subsequently, the catalyst was heated in 30 K steps until reaching 783 K. At each step, the sample was kept for 30 min and the XRD pattern was recorded in the 2θ range of 40-60º, where the most intense reflections of Ni and NiO appear. Measurements were done at a step size of 0,05º and a rate of 2 s per scan using a Bruker-AXS D8 Advance powder X-ray diffractometer equipped with a CoKα radiation (λ =1.79 Å) source.

N_2 adsorption-desorption measurements were performed on a Quadrasorb SI at 77 K to determine the specific BET area and average pore size of the samples. Before measurement, the samples were degassed overnight at 383 K. Specific surface area was determined by applying the BET method and the pore size distribution was estimated from the BJH method.

TEM characterization was done using JEOL 1011 transmission electron microscope operating at an accelerating voltage of 100 kV and magnification of 200

k. Sample (0.1 mg) was dispersed in ethanol (50 μL) with the aid of an ultrasounds. Then, it was deposited on a carbon coated copper grid and air dried.

Metallic area was determined from H_2 chemisorption experiment using an Autochem AC2920 Micrometric apparatus. In a typical experiment, 0.3 g of pre-reduced sample was re-activated by reduction under hydrogen flow at 623 K for 1 h and flushed with helium (40 mL/ min) for 30 min and cooled down to 313 K. Pulses of hydrogen were injected until saturation. The sample was purged with helium to remove the excess hydrogen. The number of metal active sites was proportional to the number of hydrogen atoms irreversibly chemisorbed and was obtained from the linear portion of the isotherm by extrapolating to zero pressure. The number of surface nickel atoms was calculated by assuming spherical particles and a stoichiometric factor of 1 corresponding to 1 hydrogen atom per each exposed Ni atom. The atomic cross sectional area of Ni and the density per atom used in the calculation were, 0.065 nm^2 and 8.9 g/cm^3, respectively. The % of metal dispersion (MD= (metallic nickel atoms on surface/total nickel atoms) * 100), was calculated from the metallic area and the atomic cross sectional area of Ni.

The reduction profiles of the catalyst precursors were obtained by TPR analysis carried out on an Autochem AC2920 Micrometric apparatus. About 100 mg sieved catalyst precursor sample was kept in a U-shaped quartz tube and purged with pure He for 30 min at 373 K and cooled down to room temperature before analysis. The analysis was carried out using a 5% H_2/Ar gas flowing at 20 mL/min by heating from room temperature to 1173 K at a heating rate of 10 K/min. A TCD detector monitored the amount of hydrogen consumed.

Surface acidity of the catalyst precursors was determined from thermogravimetric analysis (TGA) of the samples treated with cyclohexylamine (CHA) following the protocol described by Mokaya *et al* [45]. About 0.1 g of sample was covered

completely with CHA with the help of a pasture pipette. The excess of CHA was removed by letting it to stand on the hood overnight. TGA of the CHA-treated sample was obtained by heating the sample, under N_2 flow (80 mL/ min) from 303 to 1173 K at a rate of 10 K/ min, in a Labsys Setaram TGA microbalance equipped with a temperature programmable furnace. The TGA profile of the catalyst precursor without CHA was obtained in the same way and was subtracted as a baseline from the corresponding TGA of the CHA-treated sample. The acidity, corresponding to the more accessible acid sites, was equivalent to the amount of CHA desorbed in the temperature range of 473-923 K [44].

The total surface acidity of the catalyst precursors was determined by NH_3-TPD experiment conducted on AC2920 apparatus. In a typical experiment, about 0.2 g, sieved catalyst precursor sample was loaded in U-shaped quartz tube and submitted to surface pre-treatment under a flow of He at 623 K for 1 h. It was then cooled down to 373 K and saturated with pure NH_3 for 30 min. The physically adsorbed NH_3 was removed by purging the sample with pure He for 30 min and the sample was heated from 373 to 973 K at a heating rate of 10 K/min and the NH_3 desorption was monitored with a TCD detector. The peak area of detected TPD peak was correlated with the amount of desorbed NH_3 on the basis of pulsed NH_3 injection experiment and the total surface acidity was predicted from the amount of ammonia desorbed.

2.3. Catalytic activity test

Hydrogenolysis of glycidol was tested in a 50 mL stainless steel autoclave equipped with an electronic temperature controller and a mechanical stirrer. Glycidol (3.77 mL) was dissolved in sulfolane (30 mL) and purged with N_2. A powdered freshly reduced catalyst (1 g) was carefully transferred to the reactor under positive nitrogen pressure

to avoid contact with atmosphere. The reactor was sealed and purged three times with 2 MPa N_2 and three times with 1 MPa H_2 pressure.

A leakage test was performed, the temperature of the reaction was set at 393 K and the pressure at 1 MPa and the mixture was stirred at high rpm (600 rpm), which along with the use of powdered catalysts ensured easy mass and heat transfer and avoids internal and external diffusion problems. The influence of the reaction temperature (353, 393, 423 and 453 K) was studied for the Ni(40)/Sap catalyst. When the temperature in the electronic controller reached the reaction temperature, the hydrogen pressure was adjusted at 5 MPa and the reaction time was started (t_o). The reaction was run for 1, 2 or 4 h, while feeding hydrogen on demand. At the end of the reaction, the mixture was cooled down and gaseous reaction products were collected in a gas sample bag. The reaction products were separated from the catalyst by centrifugation and liquid products were analysed on a Shimadzu GC-2010 chromatograph using SupraWAX-280 capillary column, 1-butanol as internal standard and a FID detector. Some of the liquid samples were submitted for GC-MS analysis to identify unknown products. Conversion and selectivity were calculated according to the following equations:

$$\%Conversion = \frac{(moles\ \ t_o - \ moles\ \ t_f)}{moles\ t_o} * 100$$

$$\%\ Selectivity\ x = \frac{moles\ of\ analyte\ x}{moles\ of\ glycidol\ converted} * 100$$

Where t_o and t_f are the initial and the final times, respectively.

3. Results and discussion

3.1. Characterization of the catalyst precursors

212 XRD patterns of the catalyst precursors showed peaks at 37.2, 43.2 and 63.1 º, 2θ,
213 which were due to the NiO crystalline phase (Figure S1). Additionally, the peaks at
214 19.4, 35.6, 60.5º, 2θ, observed for all samples, were related to the (110, 020), (201)
215 and (060) reflections, respectively, of the saponite support.

216 The average NiO crystallite sizes, reported in Table 1, were calculated from the
217 peak width obtained by fitting the characteristic reflections of NiO using TOPAS 4.1
218 and applying the Scherrer equation. The catalyst precursor PNi(15)/Sap had a NiO
219 crystallite size of 9 nm. This small size should be consequence of a good dispersion
220 of the NiO phase, a basic oxide, in an acid support with high surface area. The NiO
221 crystallite size was higher when the % loading of Ni increased (30 and 40 wt %) (Table
222 1). The NiO crystallite size was also larger for the precursor supported on the Na-form
223 of the saponite (Sap*), PNi(40)/Sap* (37 nm), when compared to that observed for
224 the precursor supported on the acid form PNi(40)/Sap (26 nm). Therefore, the acidity
225 of the H-saponite seems to favour the dispersion of the NiO.

226 The N_2 adsorption-desorption isotherms of the catalyst precursors (i.e.,
227 PNi(x)/Sap) are displayed in supplementary information (Figure S2). All catalyst
228 precursors showed a type IV isotherm according to de Boer's classification and a
229 hysteresis loop similar to that of their corresponding supports [44]. The average pore
230 radius was in the mesoporous range for all the catalyst precursors with similar or
231 slightly higher values than those corresponding to the support, due to the partial
232 blocking of the smaller pores by the deposition of the NiO particles (Table 1). Catalyst
233 precursors mainly had type D hysteresis loop, independent of the wt % of Ni loading
234 or the support used. Type D hysteresis loop can be related to the presence of disordered
235 lamella particles, which can be associated with a higher degree of delamination.

236 The specific BET areas of the catalyst precursors are presented in Table 1. All the
237 catalyst precursors had lower BET area than their corresponding supports, which are

shown in parentheses in Table 1. This decrease of surface area can be explained by the partial occupation of the pores by NiO.

The BET areas of the catalyst precursors decreased when increasing the Ni loading. The highest BET area was obtained for the catalyst precursor PNi(15)/Sap (376 m^2/ g). The BET area of catalyst precursor PNi(40)/Sap* (203 m^2/g) was lower than that of the catalyst precursor supported on the H-form PNi(40)/Sap (229 m^2/g). This agrees with the higher crystallite size of NiO observed for the sample supported on the Na-saponite (Sap*) (Table 1).

The surface acidity values of the catalyst precursors are shown in Table 1. The surface acidity decreased when the NiO content increased, as expected, due to coverage of the support acid sites by NiO. PNi(40)/Sap* had the lowest acidity value of 0.37 mEq. CHA/g. This agrees with the nature of the Sap* support (Na-form).

The surface acidity values of the catalyst precursors, determined from TGA of the CHA-treated samples, are shown in Table 1. The surface acidity decreased when the NiO content increased, as expected, due to coverage of the support acid sites by NiO. PNi(40)/Sap* had the lowest acidity value of 0.37 mEq CHA/g. This agrees with the nature of the Sap* support (Na-form). The acidity values obtained by NH_3-TPD were slightly higher than those obtained from CHA desorption, but the tendency was similar (Table 1). However, some additional information about the acidity strength in the catalyst precursors, and consequently in catalysts, was obtained from the NH_3-TPD profiles (Figure 1). NiO preferentially covers the stronger acid sites of the precursors, since the minimum in the profiles shifted to lower temperature when increasing the Ni loading, This involves a decrease in the amount and strength of the acidity for the catalyst precursors in the following order (PNi(40)/Sap < PNi(30)/Sap < PNi(15)/Sap). For Ni(40)/Sap*, lower total surface acidity with weaker acid sites,

263 which might be associated to terminal –OH groups of the saponite support, was
264 observed.

265 The NiO particle sizes observed by TEM (not shown here) in the catalyst
266 precursors are also depicted in Table 1. The average particle size calculated from TEM
267 analysis was in good agreement with the average crystallite size calculated from XRD.

268 The TPR profiles of the catalyst precursor at 15 % metal loading showed the
269 presence of three reduction peaks (Figure 2A) corresponding to different degrees of
270 interaction between NiO and the support. The important contribution of the reduction
271 peaks between 900 and 1073 K explains the low reducibility observed for PNi(15)/Sap
272 although this catalyst precursor also had reduction peaks between 616 and 748 K
273 associated to NiO particles with higher reducibility.

274 The TPR profiles of PNi(30)/Sap and PNi(40)/Sap showed higher reducibility of
275 both samples than that observed for PNi(15)/Sap since the main peaks appeared below
276 900 K. However, the reducibility of PNi(30)/Sap was significantly lower than that of
277 PNi(40)/Sap, as confirmed by the shift of the main reduction peak of the later from
278 800 K to 643 K (Figure 2B and 2C). Moreover, the TPR profile of PNi(30)/Sap
279 presented peaks at 650 and 990 K corresponding to NiO particles with different
280 degrees of interaction with the support. The TPR profile of PNi(40)/Sap* catalyst
281 precursor (Figure 2D) showed that its reducibility was lower than that of PNi(40)/Sap.
282 This could most likely be related to the higher NiO particle size of the catalyst
283 precursor supported on Na-saponite (Table 1).

284 The in-situ XRD experiments, plotted on Figure 3, were conducted for
285 PNi(15)/Sap in order to gain additional information about the NiO reduction
286 temperature. The reduction of this catalyst precursor started at 623 K, then the amount
287 of metallic nickel increased and the amount of NiO decreased when increasing the
288 reduction temperature. However, the total reduction was not reached until 783 K. The

initial reduction temperature was in agreement with the first peak obtained in the profile of the TPR technique (616 K) (Figure 2A). However, it is difficult to have a good correlation at all temperatures, since the conditions of heating rate and the % of H_2 in the flow were different in both experiments.

3.2. Characterization of the catalysts

After reduction at 623 K for 6 h, XRD patterns of the catalyst Ni(15)/Sap did not show peaks at 44.5 and 51.9º, 2θ corresponding to metallic nickel (Figure 4). This could be explained by the low reducibility of the NiO in this sample. However, considering the results obtained by in situ-XRD and TPR of its precursor, some re-oxidation of small nickel particles when recording the XRD of this catalyst under air, should be also considered. On the other hand, the catalysts with higher Ni loading (30 and 40 wt %), supported on the H- or on the Na-form, showed the characteristic peaks due to metallic Ni phase (Figure 4). The Ni crystallite size in the reduced samples was slightly lower than the size of their corresponding NiO precursors.

Typical TEM images of the catalysts are displayed in Figure S3. The micrographs showed the lamellar structure of the supports together with dark spots that can be assigned to Ni or NiO nanoparticles, depending on the reduction degree. The Ni average particle size is indicated in Table 2. The Ni average particle size calculated from TEM analysis was in good agreement with the average crystallite size calculated from XRD.

The metallic area determined by H_2 chemisorption for catalysts was in agreement with the reducibility results (Table 2). Ni(15)/Sap gave the lowest Ni metallic area (< 1 m^2/ g). Probably, the small NiO particles (10 nm by TEM) interacted strongly with the acid support and thus giving a lower reducibility. A similar result was reported on

the role of TiO_2 and WO_3 acidity in enhancing the dispersion of Pt nanoparticles in $Pt/WO_3/TiO_2/SiO_2$ catalysts [47]46

The metallic area of the catalysts with 30 % and 40 % Ni loading can be correlated with the reducibility of their corresponding catalyst precursors and the resulting metal particle size. Thus, the catalyst with the highest metallic area was Ni(40)/Sap (7.5 m^2/g). The metallic area of the Ni(30)/Sap catalyst was lower (2.8 m^2/g). This result is in agreement with the important % of NiO phase observed in the diffractogram of this catalyst (Figure 4). The metallic area of the catalyst prepared using the Na form of the support was lower than that of the corresponding catalyts prepared with the acid support (Table 2), in agreement with the lower reducibility of the former. A good balance between NiO particle size and its interaction with the support favoured the best reducibility of sample in case of PNi(40)/Sap. Metal dispersion % values, shown in Table 2, were very low in agreement with the high amount of the metal loading used following the sequence (Ni(15)/Sap < Ni(40)/Sap*= Ni(30)/Sap<Ni(40)/Sap. The higher dispersion of the metal in catalyst Ni(40)/Sap agrees with its higher metallic area (7.5 m^2/g).

3.3. Catalytic activity

The catalytic activity for all the catalysts studied in this work are presented in terms of conversion, 1,2- and 1,3-PrD selectivity and 1,3-PrD/1,2-PrD ratios. Table 3 summarizes the catalytic activity results for the hydrogenolysis of glycidol. Catalyst at 15 wt. % Ni loading showed moderate activity (conversion, 46 %) with low selectivity to propanediols (30%). The selectivity to 1,2-PrD was higher than to 1,3-PrD, but the 1,3-PrD/1,2-PrD ratio was high enough (0,76). The selectivity to undesired products (named as others in Table 3) was very high for Ni(15)/Sap (70%). These other products include propanol and condensation products resulted from

338 glycidol and PrDs, according to GC-MS analysis. In fact, the formation of similar
339 condensation reaction products was reported between aldehydes or ketones and diols
340 on solid acid catalysts [48 47]. We cannot discard the contribution of other products
341 resulted from C-C cleavage or polymerization that cannot be detected in the
342 chromatogram.

343 The catalytic activity of the catalysts supported on Sap at 30 and 40 wt. % Ni
344 loading were higher than those obtained for the catalyst with 15 wt % Ni loading
345 (Table 3). Almost total conversion was obtained for the two catalysts supported on
346 Sap in the H-form (Ni(30)/Sap and Ni(40)/Sap) (Table 3). However, lower conversion
347 (73%) was obtained for the catalyst supported on the Na-form of Sap. The selectivity
348 to propanediols (1,2-PrD + 1,3-PrD) was higher for the catalysts with higher Ni
349 loading (30 and 40%), but the differences between Ni(30)/Sap, Ni(40)/Sap and
350 Ni(40)/Sap* were not significant (84, 79 and 84% respectively). The selectivity to 1,3-
351 PrD was higher for the catalysts prepared at higher Ni loading and supported on Sap
352 (20-26%). However, the 1,3-PrD/1,2-PrD ratio values were lower at 30 and 40 wt %
353 Ni loading than at 15 wt % Ni loading. The Ni(40)/Sap catalyst presented the highest
354 yield to 1,3-PrD among all the catalysts investigated in this work (26%).

355 Different catalytic reactions compete for the glycidol transformation: the metal
356 catalysed hydrogenolysis to propanediols and the acid and metal catalysed secondary
357 reactions to side-products. The low conversion and low selectivity to propanediols
358 obtained for Ni(15)/Sap catalyst might be mainly the result of its lower metal area
359 (Table 2), In contrast, its higher selectivity to others could be related to its higher
360 amount and strength of acidity. For Ni(40)/Sap*, the lower conversion should be due
361 to its lower acidity and lower metal area compared to Ni(40)/Sap. Higher selectivity
362 to propanediols should be expected for Ni(40)/Sap considering its higher metallic
363 area (7.5 m^2/ g). However, other effects should be also considered. Higher nickel

metallic area might involve higher metallic activity, increasing the hydrogenolysis capacity of Ni, but also its hydrogenating capacity and consequently, favouring the C-C cracking.

The 1,3-PrD/1,2-PrD ratio was quite high for Ni(15)/Sap catalyst. The expected high acidity of this catalyst, due to the high acidity of its precursor (Table 1) suggest that some contribution of these acid sites in the hydrogenolysis of glycidol to 1,3-PrD could be expected. We propose that the hydrogenolysis reaction can follow two different mechanisms, related to differences in the hydrogenation of C2 and C3 carbons in the glycidol (Scheme 1). In the first one, a Brønsted acid activation of glycidol through the O in the cyclic ether takes place and is followed by metal catalysed hydrogenation in the C2 and C3 carbons of the glycidol [49 48]. The other involves a direct hydrogenation on the C3 position of the less substituted carbon, without acid activation. In the former mechanism, the products are 1,2-PrD and 1,3-PrD whereas in the latter case, 1,2-PRD is the main product.

The results of 1,3-PrD selectivity and 1,3-PrD/1,2-PrD ratio of catalysts with higher Ni loading (30 and 40%), suggest also that the differences can be related to an acid activation of glycidol during hydrogenolysis, as previously commented. Considering the loss of acid sites when increasing the wt % of Ni, the acid activation should be lower. This could explain the lower 1,3-PrD/1,2-PrD ratio observed for catalysts with 30 and 40 wt % Ni loading with respect to that with 15 wt % Ni. However, it is important to remark that the ratio was higher for the catalyst with 40 wt % Ni (0.49) than that with the 30 wt % Ni (0.38). This could be a consequence of the higher dispersion of the metal Ni nanoparticles (Table 2) favouring a more effective collaborative action between metal and acid sites. From this analysis we can suggest that 1,3-PrD formation can be related to a balanced interplay between the acid and metal function of the catalysts. The beneficial effect of the acid sites was observed

by analysing the catalytic activity of the Na-form, Ni(40)/Sap* catalyst. This catalyst presented lower conversion and lower selectivity to 1,3-PrD in comparison to the corresponding catalyst prepared with the H-form of the saponite, Sap. This catalytic behaviour can be correlated with the lower acidity of this catalyst. This behaviour confirms again the contribution of acidity in the 1,3-PrD formation.

3.4. Optimization of the reaction temperature and time

After screening the catalytic materials, the influence of the reaction temperature and time was studied with the most promising Ni(40)/Sap catalyst. The effect of the reaction temperature on the hydrogenolysis of glycidol was investigated at 353, 393, 423 and 453 K for 4 h. The results, in Figure 5, revealed that at 353 K, moderate conversion (46 %), high diol selectivity (84 %) and the lowest 1,3-PrD/ 1.2-PrD ratio (0.21) was obtained. When the reaction temperature was increased to 393 K or higher, total conversion was obtained.

The diol selectivity decreased to 78% with higher 1,3-PrD/ 1,2-PrD ratio (i.e., 0.49) at 393 K compared to the results obtained at 353 K. Further increase of the reaction temperature up to 423 and 453 K decreased the propanediol selectivity to 56 and 52 %, respectively. This decrease of diol selectivity can be considered similar to that observed in the previous section when catalysts with higher metallic activity were used and was correlated with the formation of cracking products. However, the reaction temperature had a positive effect on the 1,3-PrD/1,2-PrD ratio and increased up to 0.88 at the highest reaction temperature.

As commented in previous sections, we proposed that the acid activation of glycidol could favour the formation of both propanediols (1,3-PrD and 1,2-PrD). This mechanism is favoured when the activity of the acid sites is higher. At higher reaction

temperature, the contribution of this mechanism is most likely higher, with a subsequent increase of the 1,3-PrD/1,2-PrD ratio close to 1.

In order to account for a thermal reaction contribution, a new experiment was performed at 453 K for 4 h under 5 MPa hydrogen pressure without catalyst. The resulting conversion was very low (< 2%) indicating that the contribution of thermal reaction was minimal.

In order to understand the effect of the reaction time at 453 K, we performed the reaction at the same reaction conditions but at shorter reaction time (1 and 2 h) using the Ni(40)/Sap catalyst. After the first hour, total conversion was already obtained with 30 and 29 % selectivity to 1,2-PrD and 1,3-PrD, respectively. After 2 and 4 h, the 1,2-PrD and 1,3-PrD decreased slightly to 29 and 28 % and 26 and 24 %, respectively. This decrease in the diol selectivity values could be explained by some contribution of the acid sites, over hydrogenolysis or hydrogenation side reactions of propanediols. At the optimum reaction conditions, 453 K and after 1 h, the reaction gave 30 % and 29 % selectivity, respectively, for 1,2-PrD and 1,3-PrD with total conversion. The yield of 1,3-PrD (i.e. 29%) is comparable or higher than the yield reported by other authors for the direct hydrogenolysis of glycerol using noble metal based catalysts and reactions performed at higher temperature (>453 K), longer reaction time (8-24 h) and high H_2 pressure [17-23].

4. Conclusions

The selective hydrogenolysis of glycidol to propanediols was evaluated by using Ni catalysts supported on a mesoporous acid saponite. Support acidity played an important role in NiO reducibility. The low reducibility of catalyst with 15 wt. % Ni resulted in low conversion. The increase in the amount of Ni loading to 30 and 40 wt % led to higher catalytic activity (93-100%) and lower 1,3-PrD/ 1,2-PrD ratio

compared to catalysts at 15 wt % Ni loading. The selectivity to propanediols (1,2-PrD + 1,3-PrD) was higher when the metallic area was higher and acidity was lower. The contribution of an acid activation of glycidol during the hydrogenolysis reaction could favour a similar formation of 1,3-PrD and 1,2-PrD (higher 1,3PD/ 1,2PrD ratio than without acid activation). The catalysts in the Na-form of saponite yielded lower 1,3-PrD/ 1,2-PrD ratio corroborating the importance of the acid sites in the formation of 1,3-PrD. High yield to 1,3-PrD (26%), was obtained for Ni(40)/Sap catalyst after 4 h of reaction at 353 K. The catalytic activity of Ni(40)/Sap catalyst increased from 46 % at 353 K to total conversion at higher temperatures (393, 423 and 453 K). The 1,3-PrD/1,2-PrD ratio also increased with temperature, but the PrDs selectivity decreased due to both Ni and acid catalysed side reactions. Total conversion and higher yield to 1,3-PrD (29%) was obtained when the reaction was performed at 453 K for 1 h. This yield was comparable to the result obtained for glycerol hydrogenolysis using noble metal catalysts at harder conditions. Taking into account that glycidol was reported to be obtained in 78 % yield from glycerol in 90 min, regarding our results, 1,3-PrD could be obtained in two-steps, starting from glycerol, with 23% overall yield in less than 3 h for the two steps. This 1,3-PrD yield was comparable for direct glycerol hydrogenolysis obtained using noble metal catalysts, at harder reaction conditions and longer reaction times.

Acknowledgements

The authors are grateful for the financial support of the Ministerio de Economia y Competividad of Spain and FEDER funds (CTQ2011-24610). The authors are indebted to Prof. Bert Weckhuysen for his fruitful scientific discussion on the catalytic results.

References

[1]. F. Manzano-Agugliaro, M. J. Sanchez-Muros, F. G Barroso, A. Martínez-Sánchez, S. Rojo, C. Pérez-Bañón, Renew. Sust. Energ. Rev., 16 (6) (2012) 3744–3753.

[2]. R Baños, F Manzano-Agugliaro, F. G. Montoya, C. Gil, A. Alcayde, J. Gómez, Renew. Sust. Energ. Rev., 15 (4) (2011) 1753–1766.

[3]. T.E. Bull, Science 285 (1999) 1209-1209.

[4]. B. Katryniok, S. Paul, V. Bellière–Baca, P. Rey, F. Dumeignil, Green Chem. 12 (2010) 2079-2098.

[5]. C. H. Zhou, J. N. Beltramini, Y. X. Fan, G. Q. Lu, Chem. Soc. Rev. 37 (2008) 527–549.

[6]. M. Pagliaro, R. Ciriminna, H. Kimura, M. Rossi, C. D. Pina, Angew. Chem. Int. Ed. 46 (2007) 4434–4440.

[7]. Z. Xiao, C. Li, J. Xiu, X. Wang, C. T. Williams, C. Liang, J. Mol. Catal. A: Chem. 365 (2012) 24–31.

[8]. I. Gandarias, J. Requies, P. L. Arias, U. Armbruster, A. Martin, J. Catal. 290 (2012) 79–89.

[9]. R. B. Mane, A. A. Ghalwadkar, A. M. Hengne, Y. R. Suryawanshi, C. V. Rode, Catal. Today 164 (2011) 447–450.

[10]. T. Sánchez, P. Salagre, Y. Cesteros, A. B. López, Chem. Eng. J. 179 (2012) 302– 311.

[11]. C. Julien, L. Djakovitch, P. Gallezot, P. Marion, C. Pinel and C. Rosierb, Green Chem., 2004, 6, 359–361.

[12]. P. N. Caley and R. C. Everett, Patent US 3 350 871, 1967, (DuPont).

[13]. D. Zimmerman and R. B. Isaacson, Patent US 3 814 725, 1974, (Celanese Corp).

[14]. A. Perosa, P. Tundo, Ind. Eng. Chem. Res. 44 (2005) 8535-8537.

[15]. F. Jérmôe, Y. Pouilloux, J.Barrault, ChemSusChem. 7(2008) 586-613.

[16]. G. Gottschalk, B. Averhoff, US Patent 5164309 (1992) to Unilever Patent Holdings.

[17]. E. H. Himmi, A. Bories, F. Barbirato, Bioresour. Technol. 67 (1999) 123-128.

[18]. V. Nagarajan, C. E. Nakamura, US 5821092 (1998) to Dupont.

[19]. T. Kurosaka, H. Maruyama, I. Naribayashi, Y. Sasaki, Catal. Commun., 9 (2008) 1360-1363.

[20]. T. M. Che, US 4642394 (1987), to Celanese Corp.

[21]. E. Drent, W. W. Jager, US Patent 6080898(2000), to Shell Oil Co.

[22]. M. Schlaf, P. Ghosh, P. J. Fagan, E. Hauptman, R. M. Bullock, Angew. Chem. Int. Ed. 40 (2001) 3887-3890.

[23]. J. Chaminand, L. Djakovitch, P. Gallezot, P. Marion, C. Pinel, C. Rosier, Green Chem. 6 (2004) 359-361.

[24]. Y. Nakagawa, Y. Shinmi, S. Koso, K. Tomishige, J. Catal. 272 (2010) 191–194.

[25]. Y. Amada, Y. Shinmi, S. Koso, T. Kubota, Y. Nakagawa, K. Tomishige, Appl. Catal. B: Environ. 105 (2011) 117–127.

[26]. Y. Nakagawa, X. Ning, Y. Amada, K. Tomishige, Appl. Catal. A: General 433–434 (2012) 128–134.

[27]. L. Huang, Y. Zhu, H. Zheng, G. Ding, Y. Li, Catal. Lett. 131 (2009) 312-320.

[28]. C. Montassier, D. Giraud, J. Barbier, in: Stud. Surf. Sci. Catal., ed. C. Montassier et al. Elsevier, Amsterdam (1988) 165-170.

[29]. L. Z. Qin, M. J. Song, C. L. Chen., Green Chem., 12 (2010) 1466-1472.

[30]. S. Zhu, Y. Zhu, S. Hao, L. Chen, B. Zhang, Y. Li., Catal. Lett. 142 (2012) 267-274.

[31]. K. Wang, M. C. Hawley, S. J. DeAthos, Ind. Eng. Chem. Res. 42 (2003) 2913-2924.

[32]. W. Girke, H. Klenk, D. Arntz, A. Neher, T. Hass, DE 4238492 A1 (1998) to Degussa.

[33]. G. Sienel, R. Rieth, K. T. Rowbottom, (1987) In: W. Gerhartz, Y. S. Yamamoto, L. Kaudy, J. F. Rounsaville, G. Schulz, eds., Ullmann's Encyclopedia of Chemical Technology, 5th Ed., Vol. A9, New York, Wiley-VCH Publishers, 541.

[34]. A. A. Grigor'ev, N. G. Markina, L. A. Katsman, M. I. Malnykina, V. I. Zavorotov, L. S. Pozin, Neftekhimiya 19 (1979) 803–808 (in Russian).

[35]. G. J. Hutchings, D. F. Lee, A. R. Minihan, Catal. Lett. 33 (1995) 369–385.

[36]. A. Fási, I. Pálinkó and I. Kiricsi, J. Catal., 1999, 188, 385-392.

[37]. A. Fási, I. Pálinkó and I. Kiricsi, Stud. Surf. Sci. Catal., 2000, 130, 839-844.

[38]. A. Fási, Á. Gömöry, I. Pálinkó and I. Kiricsi, J. Catal., 2001, 200, 340-344.

[39]. A., I. Pálinkó, K. Hernadi and I. Kiricsi, Catal. Lett., 2002, 81, 237-240.

[40]. M. Bartók1, A. Fási and F. Notheisz, J. Catal. 1998, 175, 40–47.

[41]. M. Bartók1, A. Fási and F. Notheisz, J. Mol. Catal. A: Chem., 1998, 135, 307–316.

[42]. S. Koso, Y. Nakagawa, K. Tomishige, J. Catal., 280 (2011) 221–229.

[43]. K. Chen, K. Mori, H. Watanabeb, Y. Nakagawaa, K. Tomishige, J. Catal., 294 (2012) 171–183.

[44]. F. B. Gebretsadik, D. Mance, M. Baldus, P. Salagre, Y. Cesteros, Appl. Clay Sci. 114 (2015) 20–30.

[45]. R. Mokaya, W. Jones, S. Moreno, G. Poncelet, Catal. Lett. 49 (1997) 87-94.

[46]. L. Gong, Y. Lu, Y. Ding, R. Lin, J. Li, W. Dong, T. Wang, W. Chen, App. Catal. A: General 390 (2010) 119–126.

[47]. M. Schlaf, Dalton Trans. 394 (2006) 4645-4653.

[48]. M. Chia, Y.J. Pagán-Torres, D.D. Hibbitts, Q. Tan, H.N. Pham, A.K. Datye, M. Neurock, R.J. Davis, J.A. Dumesic, J. Am. Chem. Soc. 133 (2011) 12675.

[49]. V. Ponec, Appl. Catal., A: Gen., 2001, 222, 31–45.

Table 1: Characterization of the catalyst precursors.

Catalyst Precursors	BET (m^2/g)	Av. pore radius (Å)	Acidity [a] (mEq /g)		NiO [b] crys. size (nm)	NiO [c] part. size (nm)
			CHA-TGA	NH_3-TPD		
PNi(15)/Sap	376 (603)	36 (35)	0.96 (1.02)	1.01	9	10
PNi(30)/Sap	318	38	0.67	1.09	18	19
PNi(40)/Sap	229	38	0.59	0.73	26	27
PNi(40)/Sap*	203 (603)	35 (35)	0.37 (0.42)	0.67	37	39

The values shown in parentheses correspond to the supports. [a]Acidity in mEq CHA/g from TGA of cyclohexylamine (CHA) and NH_3-TPD. [b]XRD, [c]TEM.

Table 2: Characterization of the catalyst.

Catalysts	Ni(NiO) [a] cry. size (nm)	Ni(NiO) [b] par. size (nm)	MSA[c] (m^2/g)	% MD[d] $*10^{-2}$
Ni(15)/Sap	7 (NiO)	8	0.9	0.84
Ni(30)/Sap	16	17	2.8	1.4
Ni(40)/Sap	23	22	7.5	2.8
Ni(40)/Sap*	35	33	3.5	1.3

[a.] XRD, [b.] TEM, [c] Metallic area from H_2 chemisorption in m^2/ g of catalyst.

[d] MD corresponds to metallic dispersion.

Table 3: Catalytic activity results on the influence of metal loading and support acidity.

Catalyst	Conversion (%)	Selectivity (%)			1,3-PrD/ 1,2-PrD	1,3-PrD yield (%)
		1,3-PrD	1,2-PrD	Others		
Ni(15)/Sap	46	13	17	70	0.76	6.0
Ni(30)/Sap	93	23	61	16	0.38	21.4
Ni(40)/Sap	100	26	53	21	0.49	26
Ni(40)/Sap*	73	20	64	16	0.31	14.6

Legends and Captions

Scheme 1: Proposed reaction pathway for the hydrogenolysis of glycidol to propanediols.

Figure 1: The NH_3 TPD profiles of catalyst precursors (a) PNi(15)/Sap (b) PNi(30)/Sap (c) Ni(40)/Sap and (d) Ni(40)Sp*

Figure 2: TPR profile of the catalyst precursors (A) PNi(15)/Sap (B) PNi(30)/Sap (C) PNi(40)/Sap (D) PNi(40)/Sap*.

Figure 3: In-situ XRD profiles in dynamic conditions and under reducing atmosphere for the catalyst precursor, PNi(15)/Sap.

Figure 4: XRD patterns of catalysts (a) Ni(15)/Sap (b) Ni(30)/Sap (c) Ni(40)/Sap (d) Ni(40)/Sap*.

Figure 5: Influence of the reaction temperature on the hydrogenolysis of glycidol using Ni(40)/Sap catalyst and reactions performed for 4 h.

Figure S1: XRD patterns of catalyst precursors (a) PNiO(15)/Sap (b) PNiO(30)/Sap (c) PNiO(40)/Sap and (d) PNiO(40)/Sap*.

Figure S2: N_2 adsorption-desorption isotherms of the supported Ni catalysts.

Figure S3: TEM micrographs of catalysts (A) Ni(15)/Sap (B) Ni(30)/Sap (C) Ni(40)/Sap (D) Ni(40)/Sap*.

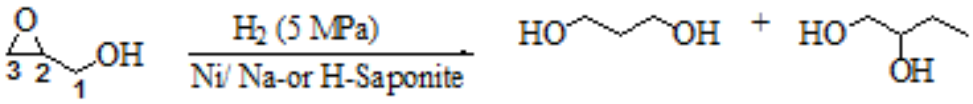

Scheme 1

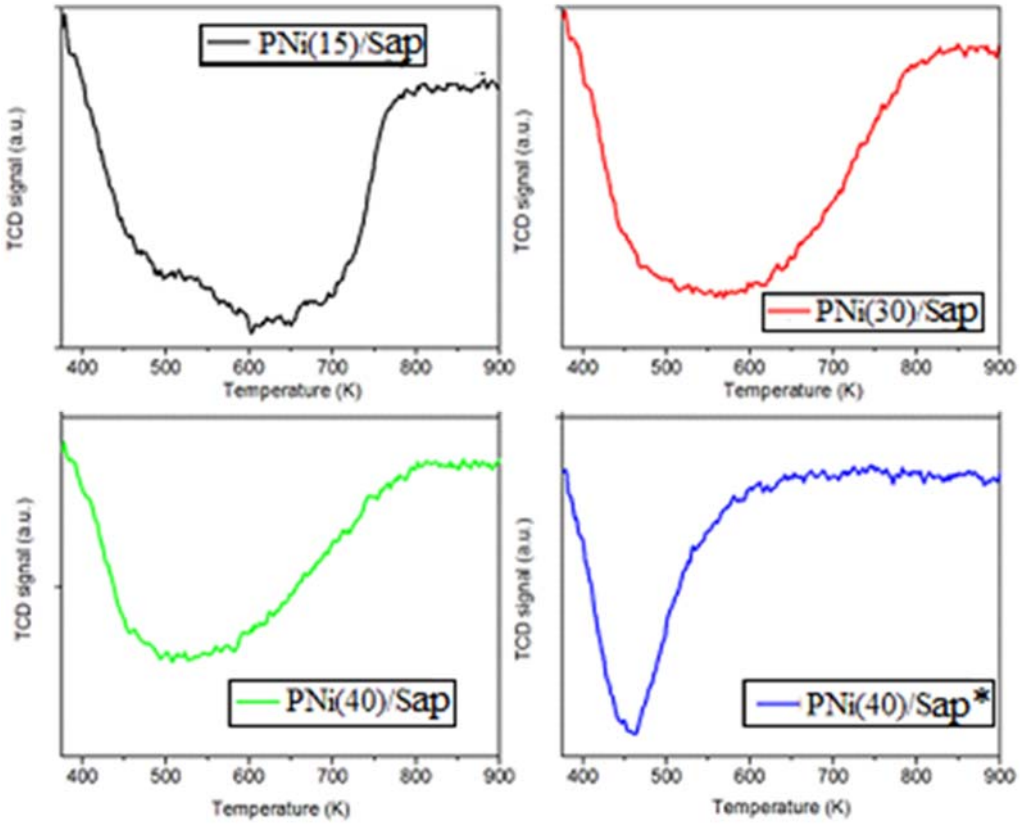
PNi(15)/Sap
PNi(30)/Sap
PNi(40)/Sap
PNi(40)/Sap*
TCD signal (a.u.)
Temperature (K)
400
500
600
700
800
900

Figure 1

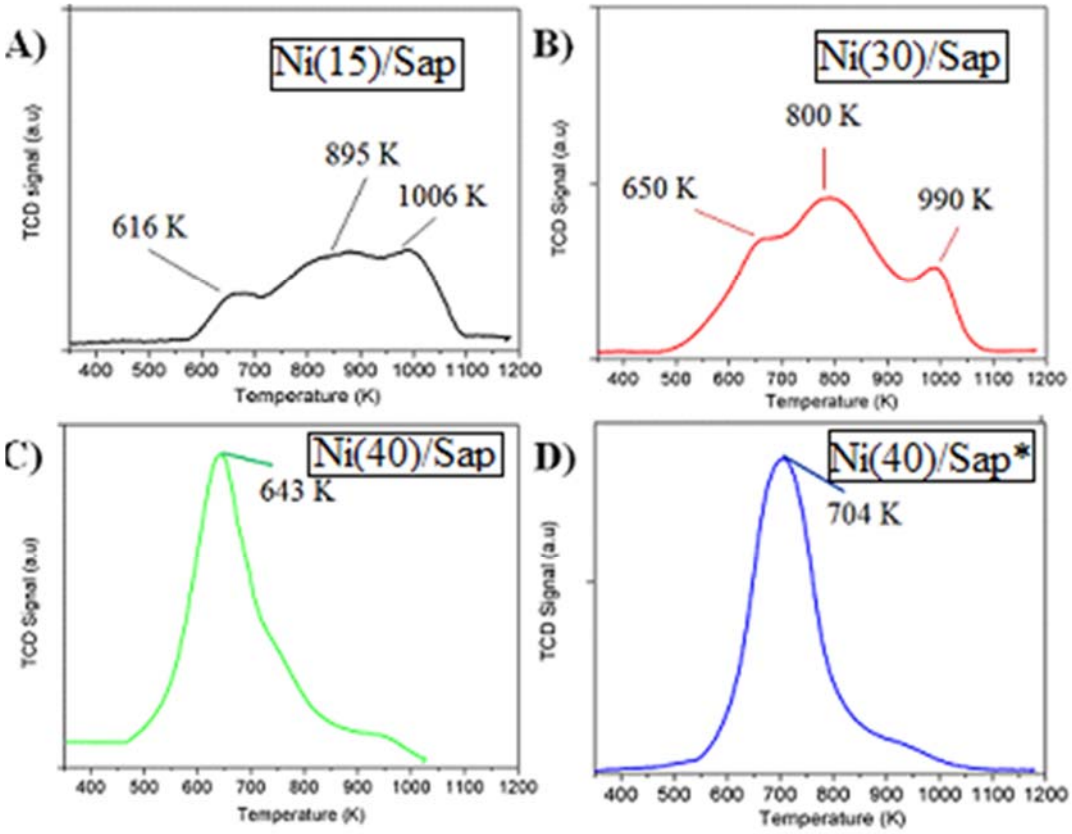
A)
Ni(15)/Sap
TCD signal (a.u)
616 K
895 K
1006 K
400 500 600 700 800 900 1000 1100 1200
Temperature (K)
B)
Ni(30)/Sap
TCD Signal (a.u)
650 K
800 K
990 K
400 500 600 700 800 900 1000 1100 1200
Temperature (K)
C)
Ni(40)/Sap
TCD Signal (a.u)
643 K
400 500 600 700 800 900 1000 1100 1200
Temperature (K)
D)
Ni(40)/Sap*
TCD Signal (a.u)
704 K
400 500 600 700 800 900 1000 1100 1200
Temperature (K)

Figure 2

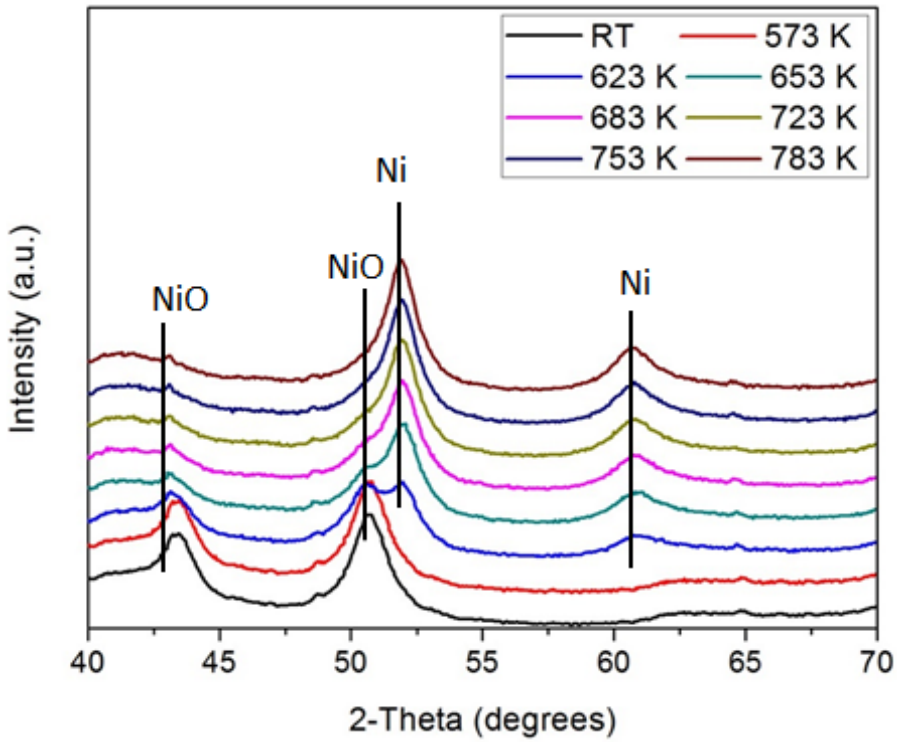
RT
573 K
623 K
653 K
683 K
723 K
753 K
783 K
Ni
NiO
NiO
Ni
Intensity (a.u.)
40
45
50
55
60
65
70
2-Theta (degrees)

Figure 3

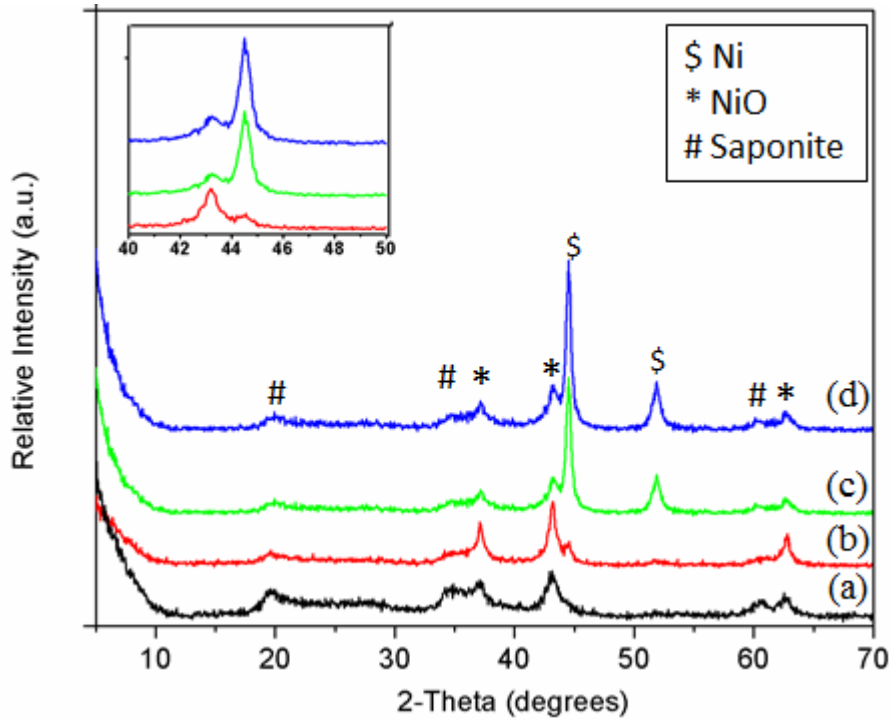
$ Ni
* NiO
# Saponite
Relative Intensity (a.u.)
2-Theta (degrees)
10
20
30
40
50
60
70
40
42
44
46
48
50
$
#
*
*
$
*
(d)
(c)
(b)
(a)

Figure 4

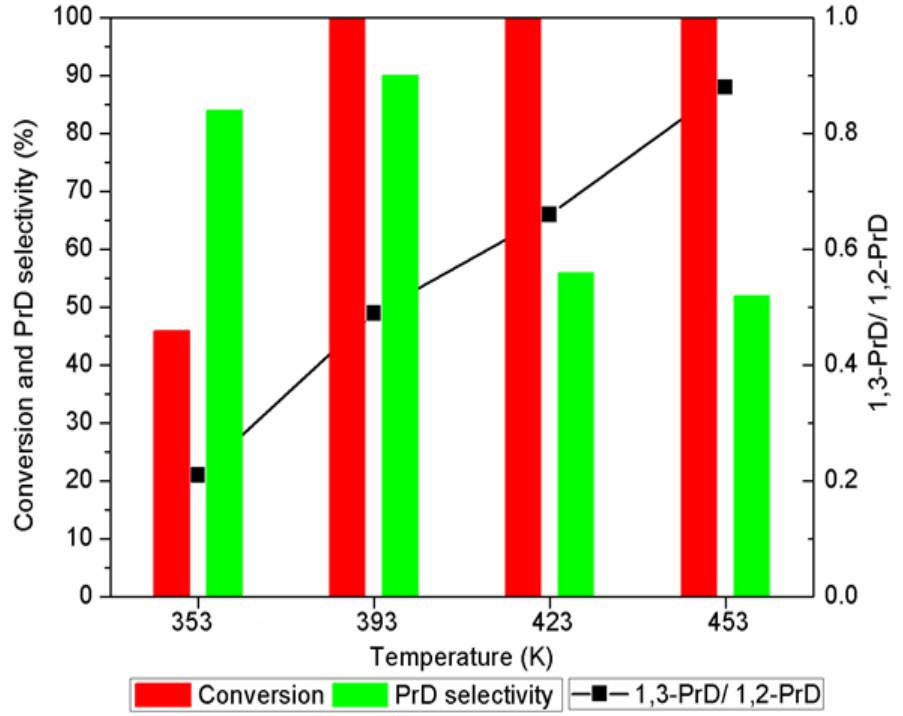
Conversion and PrD selectivity (%)
1,3-PrD/ 1,2-PrD
Temperature (K)
353
393
423
453
Conversion
PrD selectivity
1,3-PrD/ 1,2-PrD

Figure 5

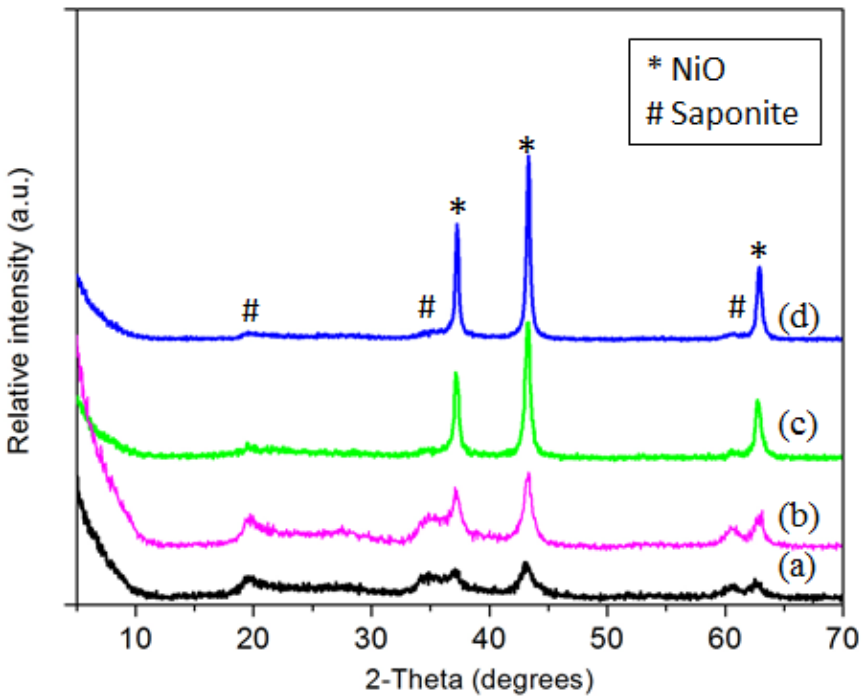
* NiO
# Saponite
Relative intensity (a.u.)
2-Theta (degrees)
10
20
30
40
50
60
70
(a)
(b)
(c)
(d)
#
#
#
*
*
*

Figure S1

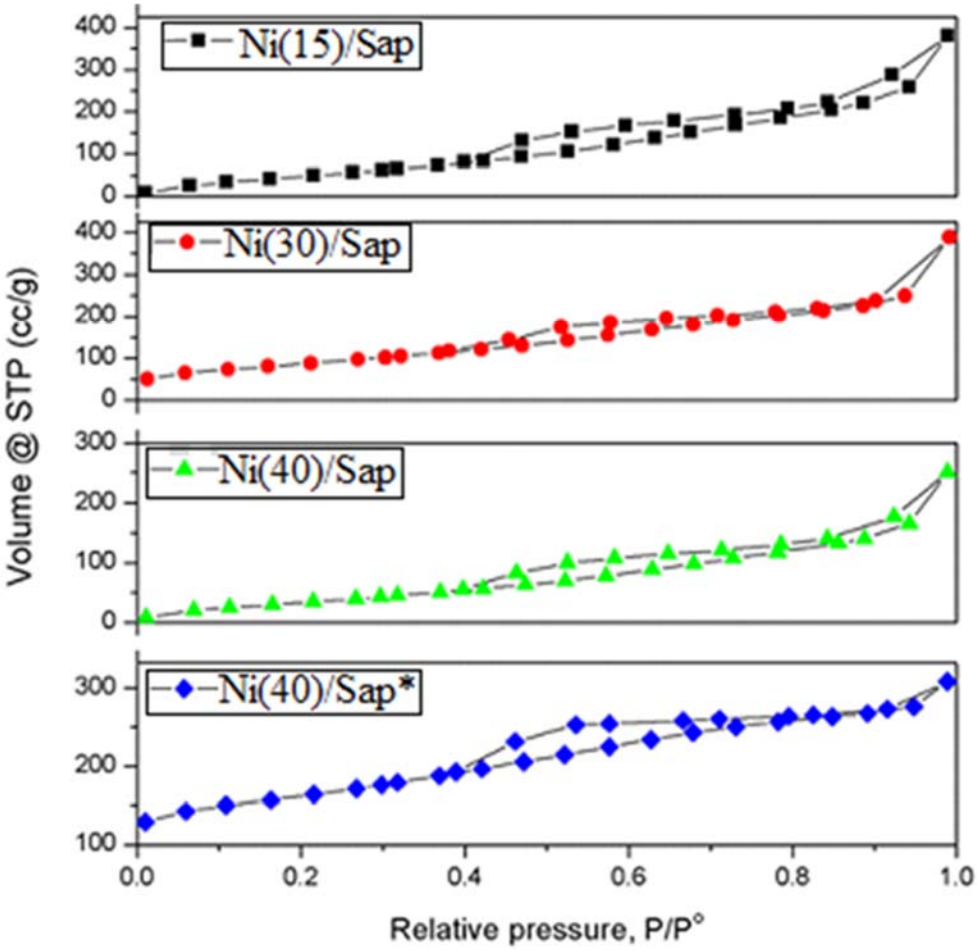
Ni(15)/Sap
Ni(30)/Sap
Ni(40)/Sap
Ni(40)/Sap*
Volume @ STP (cc/g)
Relative pressure, P/P°
0
100
200
300
400
0.0
0.2
0.4
0.6
0.8
1.0

Figure S2

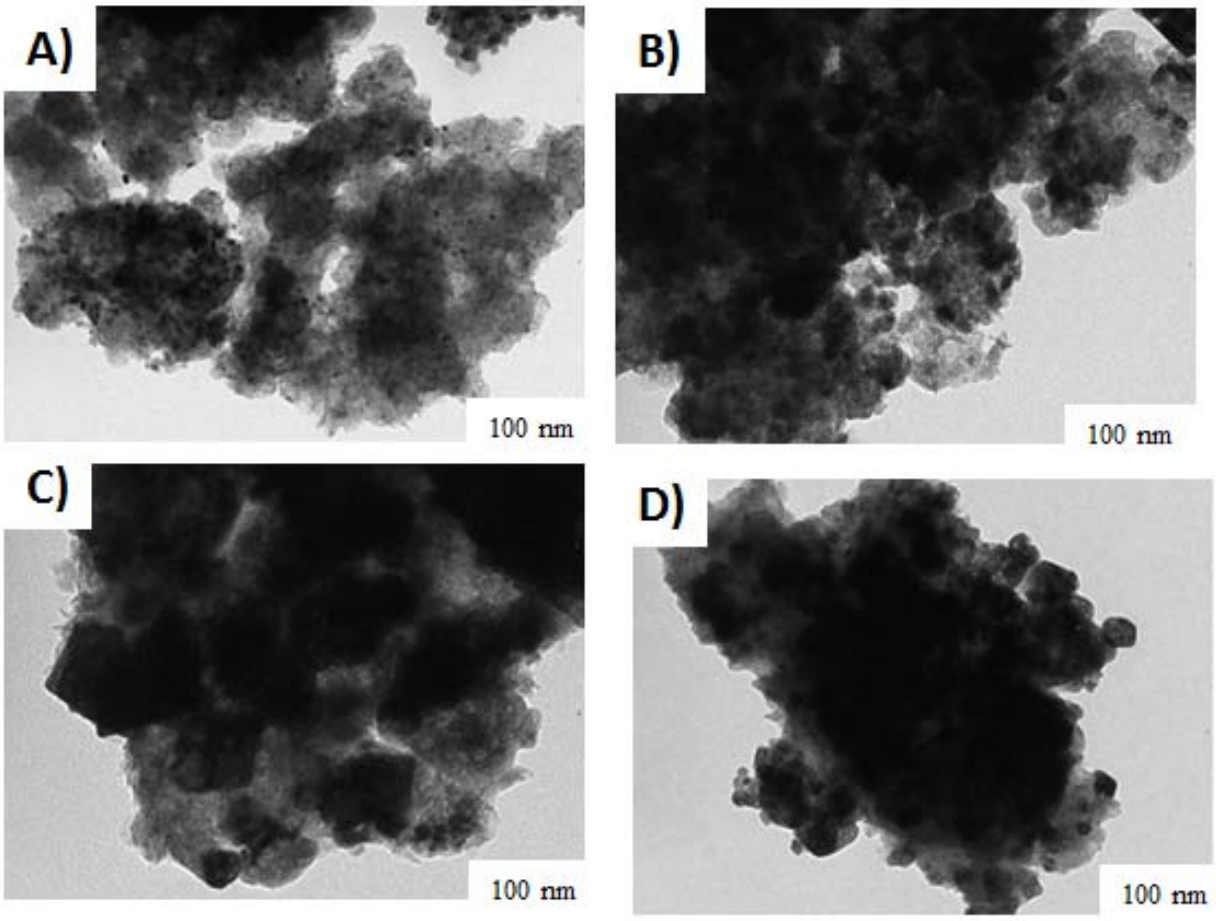

Figure S3